



Application of the BDST model for nickel removal from effluents by ion exchange

Anthony Ma^a, John P. Barford^b, Gordon McKay^{b,*}

^aHong Kong Productivity Council, Tat Chee Avenue, Kowloon, Hong Kong

^bDepartment of Chemical and Biomolecular Engineering, Hong Kong University of Science and Technology,

Clear Water Bay, Kowloon, Hong Kong

Tel. +852 23588412; email: kemckay@ust.hk

Received 18 March 2013; Accepted 12 July 2013

ABSTRACT

The effect of pH on the equilibrium ion exchange capacity of nickel using an imino diacetate ion exchange resin has been studied to determine the pH for optimum metal uptake. A series of fixed bed ion exchange studies have been carried out using the resin to remove nickel from water and the effect of a number of process variables, including initial nickel ion concentration, resin particle size and effluent solution flowrate, have been studied. The Bed Depth Service Time (BDST) model has been applied to the experimental data with only limited predictive success and subsequently a modified “BDST” model has been successfully applied to the data to model the system.

Keywords: Ion exchange; Fixed beds; Nickel ions; Imino diacetate chelating resin; Column design model

1. Introduction

Industries, like microelectronics, printed circuit board manufacturing, batteries and metal finishing, discharge large quantities of metal-bearing waste effluents, which become a major environmental problem. Toxic metals, like cadmium, copper, lead, nickel and zinc, are most commonly found in the waste effluents. Many governments have been aware of this pollution source and continue to tighten the environmental regulations [1,2].

Nickel is the metal which has received the least attention in terms of its removal from aqueous effluents. Techniques such as flotation [3], electrocoagulation [4] and liquid–liquid extraction [5] have

been used. Adsorption of nickel on several materials [6] in batch processes has been investigated including biomass [7] and other biomaterial derivatives including palm fibres [8], walnut activated carbon [9] and bone char [10,11], which has sorption and ion exchange properties. For most part the adsorption capacities for nickel are low.

Ion exchange is known to be a technique that can remove dissolved ions from the wastewater [12] and ion exchange has been used for the production of high purity water since the 1940s. Beside purification, ion exchange is also popular for the removal and recovery of materials such as radioactive wastes, toxic heavy metals and expensive metals [13].

Since ion exchange resins have a very strong affinity for dissolved ions, including heavy metals, ion exchange

*Corresponding author.

is highly suitable in purifying microelectronics waste effluents to comply with the most stringent discharge standards. The most studied natural ion exchange material for nickel removal is peat [14–19] but a modest capacity and its friability render it not very suitable for large-scale columnar operations. Nevertheless, not until the emergence of chelating ion exchange resins, purification of electroplating effluents using common ion exchange resins was still found not economical due to the rapid saturation of the ion exchange resins. The emergence of chelating resins made metal ion removal very feasible on a large scale. Chelating resins has allowed metal ions to be recovered both in single component systems and also selectively in mixed metal ion wastewaters. Some studies for batch systems have been reported. This has made the application of ion exchange in wastewater treatment increasingly popular [20–23]. Thermodynamics [24,25], mechanisms [26,27] and batch kinetics [28–30] have received considerable attention, but fixed bed column design procedures in the case of nickel have received very few studies.

In the present research, the effect of pH on the equilibrium exchange capacity for nickel has been determined using an imino diacetate chelating ion exchange resin. In addition, the application and modification of the “Bed Depth Service Time (BDST) model” to a series of fixed bed studies for the removal of nickel from water has been investigated.

2. Experimental

2.1. Chelating ion exchange resin

The iminodiacetate chelating resin sample is Suqing D401 (D401 in short) which is produced by the Jiang Yin Organic Chemical Company, Beijing, China. The resins have the iminodiacetate functional group and their initial ionic forms are di-sodium. The structure and physical characteristics of the chelating resin is shown in Fig. 1 and Table 1, respectively.

2.2. Pre-treatment of resins

According to the resin manufacturer’s information, the resin sample supplied would be in fully sodium

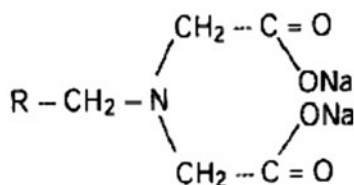


Fig. 1. Structure of iminodiacetate chelating resin.

Table 1
Physical properties of iminodiacetate resin D401

Functional group	Iminodiacetate
Ionic form	Sodium
Appearance	Opaque spheres
Bulk density, g/l	700–800
Particle density, g/l	1,150–1,250
Water retention, %	50–60
Particle size, mm	0.4–1.25 (>=95%)
Maximum operating temperature, °C	100
Total exchange capacity (Na-form), min	1.95 mmol Cu/g
Expected operating capacity (Na-form)	1.49 mmol Cu/g

*The values are copied from the technical data sheets provided by the manufacturers and are available online: <http://www.suqing.com/Engpage/production/Cation3.htm>.

form. In order to ensure consistent resin condition, the resins were treated with the standard regeneration procedures as recommended by the resin manufacturer before use for experiment. To pre-treat the resins, each resin sample was first immersed in 8% HCl (the amount of HCl would be based on a dosage of 180 g HCl per liter wet resin) for 45 min with stirring. The resin was then rinsed with deionized water to remove the residual of HCl. After that, the resin was immersed in 4% NaOH for another 45 min. Finally, the resin was rinsed with deionized water, dried and sieved to within the range of 1,000–450 μm after cooling.

2.3. Metal ion solutions

Nickel(II) chloride (NiCl_2) (98%) was supplied by Aldrich Chemicals, UK, and stock metal solutions were prepared by ultra pure deionized water. Metal ion solutions of varied concentrations were made up by diluting the stock solution with different amounts of ultra pure deionized water. Both equilibrium isotherms and a single column run were performed for copper(II) chloride and zinc(II) chloride (also from Aldrich Chemicals, UK) at a common flowrate of 180 ml/min and a common initial metal ion concentration of 1.5 mM metal ion.

With the resins prepared, the equilibrium experiments were conducted as follows: 50 ml solution of various concentrations of NiCl_2 was added into each of the 10 test bottles and a 5 ml sample was taken from the stock solution so as to measure the initial pH and initial concentration of Ni. A mass of 0.1 g D401 resin was added to each of the bottles which were then placed into the shaker bath at an agitation speed (200 rpm) and a constant temperature (22–24 °C). After agitation for 72 h until equilibrium was reached, a 5 ml sample was taken and the final concentrations of

the solutions were measured using ICP-AES. The final pH of each test bottle was measured.

The amount of metal ion sorbed, q_e , was calculated based on the following formula:

$$q_e = \frac{(C_o - C_e)V}{m} \quad (1)$$

2.4. Effect of equilibrium pH on ion exchange capacity

To investigate the pH effect on the ion exchange capacity, similar experiments were performed using different pH values.

2.5. Equilibrium isotherms

The nickel adsorption process of the iminodiacetate chelating resin is actually an equilibrium system among Na^+ , H^+ and nickel ions. Hydrolysis and protonation will take place as well during the metal ion exchange process. Thus, the solution pH will shift when the nickel ions are exchanged by the resin. When the solution pH shifts up too much, metal hydroxide precipitation will also occur. Whereas, if the solution pH shifts downward, the protonation effect becomes significant thus reducing the nickel uptake. Both metal precipitation and protonation will interfere the determination of the resin's true ion exchange capacity, and in turn distort the equilibrium isotherms. In this regard, when batch tests are used to determine equilibrium isotherms, special care should be taken to make sure that the equilibrium isotherms are not distorted by the pH shift.

2.6. Fixed bed column studies

A pilot-scale ion exchange system was built to conduct the column runs. The schematic diagram of the set-up is shown in Fig. 2. The ion exchange columns were made of Perspex tubes with an internal diameter of 2.08 cm and a height of 150 cm. The column diameter to the particle diameter ratio for this experiment ranged between 21 and 46, which was considered to be adequate such that the effects of channeling at the wall and random variations in the interstitial velocity within the bed became negligible. A retaining sieve of 65 mesh size was fixed at the bottom of the column using a special adhesive. Ballotini balls of 2 mm diameter were placed at the column bottom before putting in the resin. Points of five samples were located at 0, 20, 40, 60 and 80 from the column bottom along the straight height of the

column. Each point was sealed using Suba-seals. Five syringes of 5 cm³ were used to collect samples from these sampling points for analysis.

The nickel ion solution was delivered to the holding tank where the solution was pumped to each column via a rotameter. The rotameters would be used to monitor the flowrate which should be maintained constant throughout the experiment.

To start the experiment, the nickel ion solution in the holding tank would be pumped at constant flowrate to the ion exchange columns. Samples were taken along the column at time intervals ranging from 30 min to half an hour until the metal ion concentration of the effluent coming out from the column bottom reached the breakthrough point.

2.7. Analytical techniques

The concentrations of nickel and sodium ion solutions were measured by inductively coupled plasma-atomic emission spectrophotometer (ICP-AES). Three calibration standards and blank solution were used to form four points to establish the calibration curve for the equipment. The calibration standards were prepared using the standard solutions which were certified by the supplier. The samples were automatically measured three times in one aspiration. If the standard deviation of test results was greater than 1%, the samples were measured again until the test results fulfilled the analysis requirement.

3. Modelling

3.1. BDST design model

The BDST model has been developed from the work of Bohart and Adams [31]. In their study on the adsorption of chlorine and hydrogen chloride on charcoal, the diminishing rate of the absorbent's adsorption capacity is given by:

$$\frac{\partial N}{\partial t} = -kNC \quad (2)$$

while the solute concentration diminishes at a rate given by:

$$\frac{\partial C}{\partial Z} = -\frac{k}{u}NC \quad (3)$$

By integrating Eqs. (2) and (3), the relationship between bed depth and the time taken for breakthrough to occur is derived as follows:

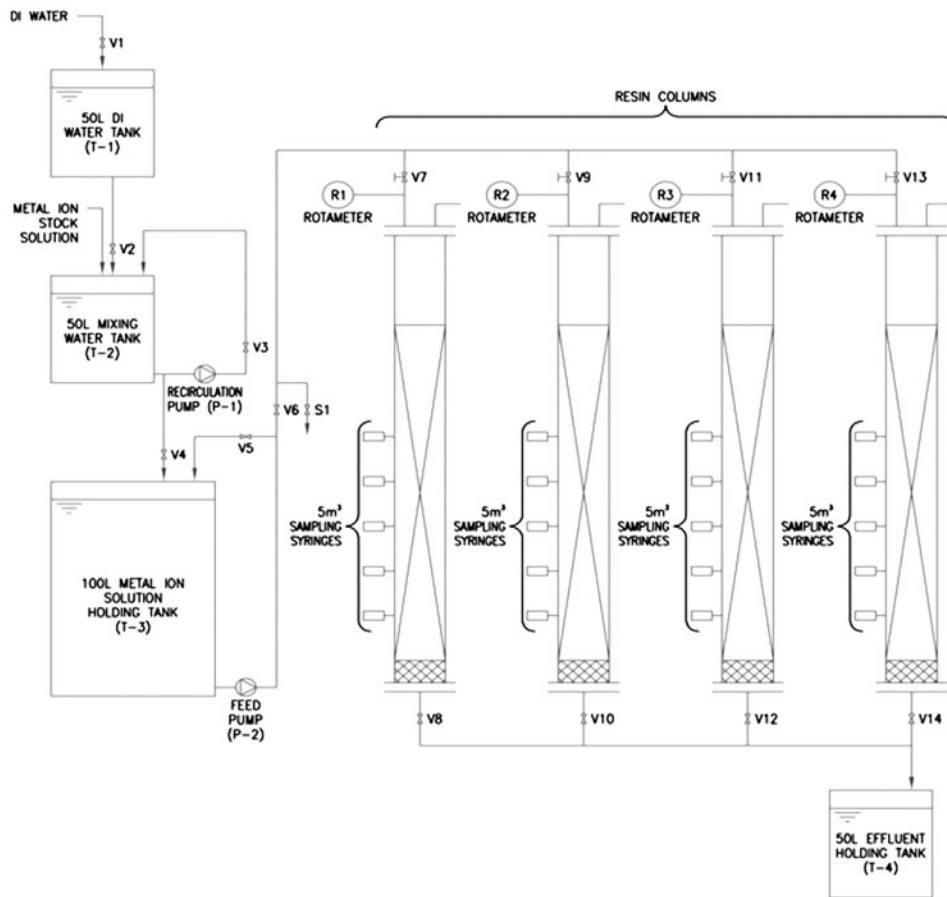


Fig. 2. Schematic diagram of the experimental system.

$$\ln\left(\frac{C_0}{C_b} - 1\right) = \ln(e^{kN_0Z/u} - 1) - kC_0t_s \quad (4)$$

$$m = \frac{N_0}{C_0u} \quad (7)$$

Hutchins [32] modified the BDST model by neglecting the unity term within the brackets on the right-hand side of Eq. (4) because $e^{kN_0Z/u}$ is usually $\gg 1$. He proposed a linear relationship between the bed depth and service time:

$$c = -\frac{1}{kC_0} \ln\left(\frac{C_0}{C_b} - 1\right) \quad (8)$$

$$t_s = \frac{N_0Z}{C_0u} - \frac{1}{kC_0} \ln\left(\frac{C_0}{C_b} - 1\right) \quad (5)$$

The “best-fit” values of m and c can be determined by minimizing the sum of error squares (SSE) between experimental data and calculated values of t_s using the built-in function “Solver” of Microsoft Excel.

Eq. (5) correlates the service time, t_s and the bed depth, Z_0 with the process parameters, including the operating flowrate, initial feed concentration, the resin exchange capacity and the sorption rate constant. Eq. (5) has the form of a straight line and can be represented by:

The critical bed depth (Z_0) is the theoretical depth of resin column sufficient to prevent the effluent metal ion concentration from exceeding C_b at $t_s=0$. By putting $t_s=0$ in Eq. (6), Z_0 is obtained from Eq. (6):

$$Z_0 = -\frac{c}{m} = \frac{u}{kN_0} \ln\left(\frac{C_0}{C_b} - 1\right) \quad (9)$$

$$t_s = mZ + c \quad (6)$$

3.2. Modification of BDST model

where the slope and y -intercept are:

The original BDST model assumes irreversible equilibrium isotherm and ignores any mass transfer

resistance during the adsorption process. So, the adsorption zone is assumed to move at a constant speed along the column and the bed adsorption capacity, N_0 , will be a constant throughout the bed. However in reality, mass transfer may play an important role in the adsorption process and the BDST plot may show a non-linear relationship. In this case, Eq. (5) may not work well. It is particularly true for those sorption cases that require long time to reach equilibrium.

In the original linear correlation between bed depth and service time, the slope of the BDST plot is equal to N_0/C_0u which has to be constant throughout the column. If the BDST plot now becomes non-linear, it should be the bed loading N_0 that has changed since both of the feed concentration, C_0 and the linear velocity, u remain constant during the course. Ko et al. [33] assumed a square-root time dependence of the bed loading and proposed the following correlation:

$$N_t = N_0(1 - \exp(-a\sqrt{t_s})) \quad (10)$$

where a is an empirical rate parameter depending on the mass transfer resistances.

The constant bed loading term, N_0 in the original BDST model, Eq. (5) is substituted by the variable, N_t as expressed in Eq. (10). The modified BDST model becomes:

$$t_s = \frac{N_0(1 - \exp(-a\sqrt{t_s}))}{C_0u}Z - \frac{1}{kC_0} \ln\left(\frac{C_0}{C_b} - 1\right) \quad (11)$$

Eq. (11) can be rearranged into the form of:

$$t_s = m'(1 - \exp(-a\sqrt{t_s}))Z + c' \quad (12)$$

where

$$m' = \frac{N_0}{C_0u} \quad (13)$$

$$c' = -\frac{1}{kC_0} \ln\left(\frac{C_0}{C_b} - 1\right) \quad (14)$$

The “best-fit” values of m' , a and c' can be determined by minimizing the SSE between experimental data and calculated values of t_s using the built-in function “Solver” of Microsoft Excel.

The critical bed depth (Z_0) now becomes:

$$Z_0 = \frac{-c'}{m'(1 - \exp(-a\sqrt{t_s}))} \quad (15)$$

4. Discussion

4.1. Equilibrium studies

The effect of pH on the exchange capacity of the resin was carried out for nickel ions and the results are shown in Fig. 3. Exchange capacities are shown in Table 2. Because of the weak acidity of the functional group, the resin shows high affinity toward hydrogen ions, i.e. protonation. As a result, as illustrated from Fig. 4, the metal ion uptake by the fully sodium form resin is drastically reduced when the equilibrium pH drops below 4.5 for the exchange of Ni ions.

Fig. 3 shows that the chelating resin has different affinity for the nickel ions at various pH values. This effect depends on the general selectivity sequence of the IDA chelating resins for different metal ions and the stability constants of the metal-iminodiacetate complexes [34–36]. The resin’s metal-ion selectivity will also be governed by a number of factors, such as the steric property of the functional group, cross-linking, hydrophobicity of the polymer matrix and extent of hydrogen bonding [22].

4.2. Equilibrium isotherm modeling

Several theoretical and empirical equations, including Langmuir, Freundlich, Langmuir–Freundlich (LF) and Redlich–Peterson (RP) isotherms were tested to fit into the experimental equilibrium data for each metal ion. The isotherm equations have been presented previously [22]. Fig. 3 shows the equilibrium isotherm for Ni and the constants of all the equilibrium isotherms are summarized in Table 3. Both the Langmuir isotherm and RP isotherm give the minimum SSE between the experimental and theoretical data with the RP giving the slightly better fit to the data. The b_{RP} of RP isotherm is equal to 0.97, which means that RP isotherm is basically very similar to the Langmuir isotherm, in which case b_{RP} is equal to unity.

4.3. BDST model bed performance with different metal ions

4.3.1. Original model

BDST plots for Ni, Cu and Zn in Fig. 5 shows very similar characteristics, which means that the bed

Table 2
Exchange capacities of nickel ions with different pH

pH	Exchange capacity q (mmol/g)					
	2.0	2.8	3.5	4.0	4.55	4.75
q	0.08	1.05	1.90	2.10	2.18	2.22

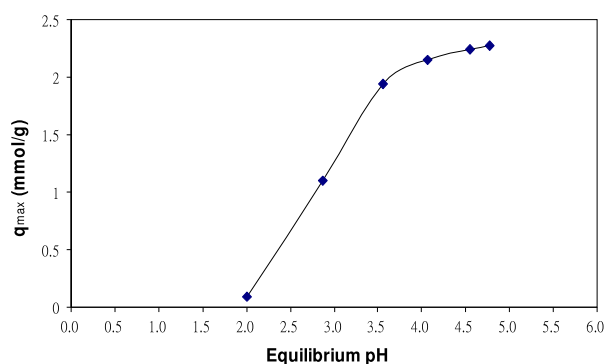


Fig. 3. Effect of equilibrium pH on the sorption of Ni by the fully sodium form of resin.

Table 3
Equilibrium isotherms for Ni on resin

Langmuir isotherm				
Metal ion	K_L	a_L		SSE
Ni	483	220		0.035
Freundlich isotherm				
Metal ion		a_F	b_F	SSE
Ni		2.17	0.02	0.069
LF isotherm				
Metal ion	K_{LF}	a_{LF}	b_{LF}	SSE
Ni	404	243	0.95	0.035
RP isotherm				
Metal ion	K_{RP}	a_{RP}	b_{RP}	SSE
Ni	482	220	0.97	0.033

performance for the three metal ions will be quite similar. From the slope, m , and the y -intercept, c , of the three lines (Table 4), volumetric bed capacity, N_o ,

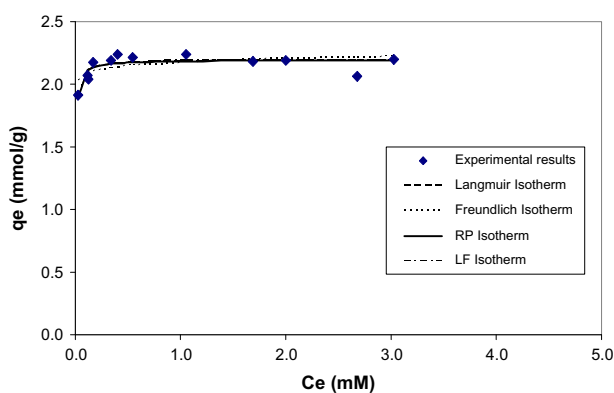


Fig. 4. Equilibrium isotherms for Ni and the fully sodium form of resin.

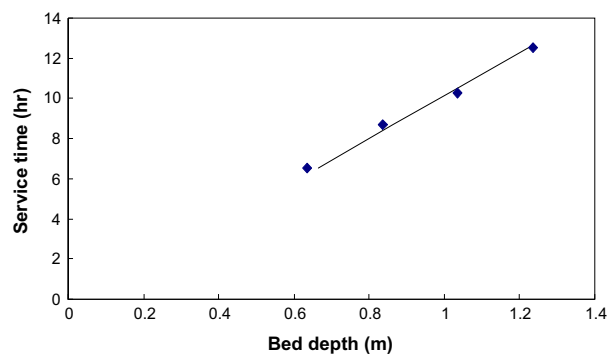


Fig. 5. BDST plot for Ni ($C_o = 1.5$ mM, mean $d_p = 725$ μ m, flowrate = 180 ml/min, 10% breakthrough).

and critical bed depth, Z_o , are calculated according to Eqs. (9) and (10), respectively. The total error of the experimental points is $\pm 8\%$ decreasing to $\pm 5\%$ with increasing time, based on a $\pm 2\%$ accuracy of concentration measurements, a $\pm 2\%$ accuracy of diluting samples and $\pm 4\%$ decreasing to $\pm 1\%$ accuracy of time in taking samples.

N_o for the nickel BDST system is 34.0 g/l and may be compared with the saturation exchange capacity derived from the equilibrium isotherm of 1.9 mmol/g. If the volumetric bed capacity, N_o , is converted to capacity based on resin dry weight by dividing N_o with the bed density, there is a discrepancy in the range of 15% between the BDST capacities and the equilibrium saturation capacities. This is consistent to many previous studies that demonstrated such a discrepancy of sorption capacities between batch and fixed-bed studies [37–39]. The discrepancy can be explained by the fact that unlike batch equilibrium studies, the residence time in the column is not long enough for the resin to reach equilibrium. Factors affecting the degree of equilibrium attained in the columns include the flowrate, initial concentration, particle size and bed depth. These factors will be discussed in detail in the following sections.

4.3.2. Modified model

Using the modified BDST model of Eq. (14), it is found that there is an improvement of 7–13% in the SSE, which implies a better fit of the model plot to the experimental data. Comparing Tables 4 and 5, both models show consistent trends in the model parameters, including the slope, y -intercept, Z_o , N_o and k . In the modified BDST model, the constant, a , is introduced to take into account the increase of bed capacity with the increase in the bed service time. Thus, the constant, a , is a rate parameter depending on the mass transfer resistance.

Table 4

BDST analysis for different metal ions ($C_o = 1.5$ mM, mean $d_p = 725$ μ m, flowrate = 180 ml/min, 10% breakthrough)

Metal ion	Slope, m (h/m)	Y-intercept, c (h)	X-intercept, Z_o (m)	N_o (g/l)	k (l/mg/h)	BDST capacity (mmol/g)	SSE ($\times 10^{-3}$)
Ni	10.7	-0.60	0.06	34.0	0.04	1.7	2.68
Cu	11.6	-1.30	0.11	36.0	0.02	1.5	0.86
Zn	10.2	-0.23	0.02	32.4	0.10	1.4	1.22

Table 5

Modified BDST analysis for different metal ions ($C_o = 1.5$ mM, mean $d_p = 725$ μ m, flowrate = 180 ml/min, 10% breakthrough)

Metal ion	m' (h/m)	c' (h)	a ($h^{-0.5}$)	Z_o (m)	N_o (g/l)	k (l/mg/h)	SSE ($\times 10^{-3}$)	New SSE/old SSE
Ni	8.6	-0.23	1.54	0.02	33.0	0.10	2.46	0.92

4.3.3. Effects of changing system variables on the BDST model

4.3.3.1. *Change of flowrate.* The effect of changing the flowrate on the bed performance for the three metal ions is analysed using both the original and modified BDST models. The results are shown in Tables 6 and 7, respectively. In general, there is an improvement in the SSE which can be up to 54% improvement when using the modified BDST model of Eq. (10). That means a better fit of the model plot to the experimental data. Comparing Tables 6 and 7, both models show consistent trends in the model parameters, including the slope, y -intercept, Z_o and N_o . As the modified BDST model gives a better data correlation, the analysis of bed performance with different flowrates will be based on the modified BDST model. The modified BDST plot for Ni ion exchange with different flowrates is shown in Fig. 6 to illustrate the effect on bed performance.

Eq. (11) shows that the BDST slope parameter, m' , is inversely proportional to the linear velocity of the liquid flow inside the fixed bed. Therefore, for a fixed C_o , if the bed capacity, N_o , is similar for columns with various flowrates, the ratios of the slope parameters will basically follow the inverse proportional relationship:

$$\frac{m'_1}{m'_2} = \frac{u_2}{u_1} \quad (16)$$

Using the BDST plot of 180 ml/min as the reference case, it is found that the prediction of the slope parameters for other flowrates by means of the above equation works quite well due to the fact that N_o is fairly constant for different flowrates.

The rate constant, a , is related to the mass transfer resistances which are basically the external mass transfer resistance and the intraparticle mass transfer resistance. For external mass transfer resistance, according to the correlation of Wilson and Geankoplis [39],

$$J_D = \frac{1.09}{\varepsilon} Re^{-2/3} \quad (17)$$

for $0.0016 < Re < 55$ where J_D is the external mass transfer coefficient.

Thus, $a \propto [Re]^{2/3}$. As $Re = \frac{\rho v d_p}{\mu}$,

$$\frac{a_1}{a_2} = \left(\frac{u_1}{u_2} \right)^{2/3} \quad (18)$$

For intraparticle mass transfer, McKay [40,41] suggested that a could be generally correlated with the square-root of the residence time, i.e. $a \propto [t']^{0.5}$. Since the residence time, t , is inversely proportional to the flowrate,

$$\frac{a_1}{a_2} = \left(\frac{t'_1}{t'_2} \right)^{0.5} = \left(\frac{u_2}{u_1} \right)^{0.5} \quad (19)$$

Combining the two effects, the correlation of a to the flowrate will be:

$$\frac{a_1}{a_2} = \left[\left(\frac{u_2}{u_1} \right)^{0.5} \right]^p \left[\left(\frac{u_2}{u_1} \right)^{-2/3} \right]^q = \left[\frac{u_2}{u_1} \right]^r \quad (20)$$

$$\text{where } \begin{cases} p + q = 1 \\ 0.5p - 2/3q = r \end{cases}$$

Based on the a values in Table 7, $r = -0.667$. Thus, p and q are 0 and 1, respectively. This suggests that

Table 6
BDST analysis for different volumetric flowrates ($C_o = 1.5 \text{ mM}$, mean $d_p = 725 \mu\text{m}$, 10% breakthrough)

Metal ion	Volumetric flowrate (ml/min)	Slope, m (h/m)	Y-intercept, c (h)	X-intercept, Z_o (m)	N_o (g/l)	SSE ($\times 10^{-3}$)
Ni	120	16.6	-0.02	0.00	35.0	0.32
Ni	140	14.1	-0.12	0.01	34.8	1.36
Ni	180	10.7	-0.60	0.06	34.0	2.68
Ni	220	8.8	-0.97	0.11	34.2	0.71

Table 7
Modified BDST analysis for different volumetric flowrates ($C_o = 1.5 \text{ mM}$, mean $d_p = 725 \mu\text{m}$, 10% breakthrough)

Metal ion	Volumetric flowrate (ml/min)	m' (h/m)	c' (h)	a ($\text{h}^{-0.5}$)	Z_o (m)	N_o (g/l)	SSE ($\times 10^{-3}$)	New SSE/old SSE
Ni	120	16.4	0.35	1.23	-0.02	34.5	0.27	0.83
Ni	140	13.9	0.20	1.32	-0.02	34.3	1.25	0.92
Ni	180	10.5	-0.30	1.54	0.03	33.3	2.46	0.92
Ni	220	8.6	-0.61	1.55	0.07	33.3	0.55	0.78

the change of bed capacity with the flowrate variation is basically due to the change of the external mass transfer resistance. As an example, the effect of a on the bed capacity for the nickel ion exchange is shown in Fig. 7.

The critical bed depth, Z_o , is found to be directly proportional to the flowrate as indicated in Eq. (13). For large flowrates, the residence time available for an ion exchange process to take place is less and thus, greater minimum bed depth is required to keep effluent concentration to below the 10% breakthrough limit. Some systems show negative Z_o such as the exchange of Ni ions with liquid flowrate of 120 ml/min. This can be interpreted as the case that at $t=0$, the bed depth, Z , is

always above the minimum bed depth required to keep the effluent concentration to below the 10% breakthrough limit.

Change of flowrate will affect the rate constant, k , which will in turn influence the y -intercept. On one hand, an increase in fluid velocity can help reduce the external film diffusion resistance (i.e. increasing k). On the other hand, a high flowrate reduces residence time, which hinders the attainment of equilibrium (i.e. decreasing k). Thus, due to opposing effects of various factors, it becomes complicated to predict the variation of k and the y -intercept.

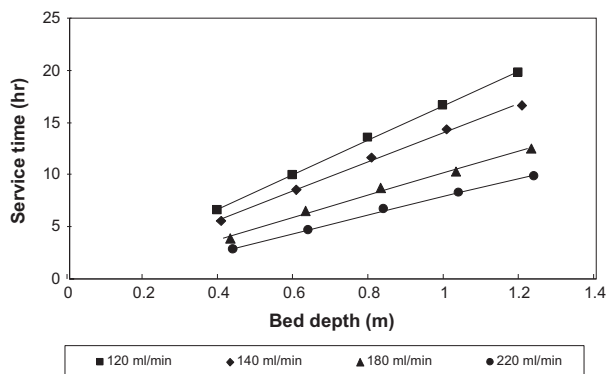


Fig. 6. Modified BDST plot for Ni ion exchange with different flowrates ($C_o = 1.5 \text{ mM}$, mean $d_p = 725 \mu\text{m}$, 10% breakthrough).

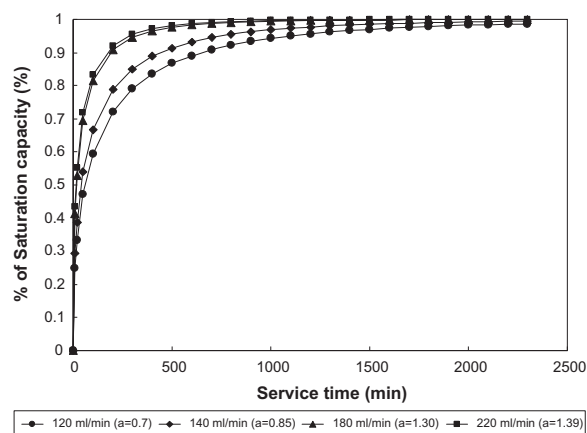


Fig. 7. Change of bed capacity for Ni ion exchange at different flowrates ($C_o = 1.5 \text{ mM}$, mean $d_p = 725 \mu\text{m}$, 10% breakthrough) $a = 1.23$ $a = 1.32$ $a = 1.54$ $a = 1.55$.

Table 8
BDST analysis for different feed concentrations (flowrate = 180 ml/min, mean $d_p = 725 \mu\text{m}$, 10% breakthrough)

Metal ion	C_o (mM)	Slope, m (h/m)	Y-intercept, c (h)	X-intercept, Z_o (m)	N_o (g/l)	SSE ($\times 10^{-3}$)
Ni	1.0	14.4	-0.02	0.01	28.0	1.39
Ni	1.7	10.3	-0.18	0.02	32.5	3.11
Ni	2.1	8.9	-0.20	0.02	34.8	1.05

Table 9
Modified BDST analysis for different feed concentrations (flowrate = 180 ml/min, mean $d_p = 725 \mu\text{m}$, 10% breakthrough)

Metal ion	C_o (mM)	m' (h/m)	c' (h)	a ($\text{h}^{-0.5}$)	Z_o (m)	N_o (g/l)	SSE ($\times 10^{-3}$)	New SSE/Old SSE
Ni	1.0	14.3	0.17	1.44	-0.01	27.8	1.29	0.93
Ni	1.7	10.1	0.10	1.45	-0.01	32.0	2.91	0.94
Ni	2.1	8.8	-0.05	1.90	0.01	34.5	0.98	0.94

4.3.3.2. *Change of feed concentration.* Tables 8 and 9 show the bed performance with different feed concentrations for the three metal ions based on original and modified BDST models, respectively. In general, there is an improvement in the SSE of up to 54% when using the modified BDST model. That means a better fit of the model plot to the experimental data. As the modified BDST model gives a better data correlation, the analysis of bed performance with different feed concentrations will be based on the modified BDST model. Fig. 8 shows the modified BDST plot for Ni ion exchange with different feed concentrations. Modified BDST plots for the other two metal ions also give a very similar shape.

From Eq (11), it can be seen that change of C_o will alter the slope parameter of the modified BDST plots. With a fixed flowrate, if N_o is assumed to be constant for columns with different feed concentrations, the slope parameter, m' , of BDST plots will be inversely proportional to C_o :

$$\frac{m'_1}{m'_2} = \frac{C_{o2}}{C_{o1}} \quad (21)$$

From Table 9, it is found that the above equation gives quite a good prediction of the slopes for different C_o due to the fact that N_o is fairly constant for all the columns. However, it is hard to predict the y-intercept from the variation of C_o because the rate constant, k , is not always constant and will influence the y-intercept.

As shown in Table 9, the rate constant, a , increases with increase in feed concentration. Since the mass transfer depends on the mass transfer coefficient and the concentration gradient, a higher feed concentration will provide a greater concentration gradient and in turn enhance mass transfer.

The empirical relationship between the rate constant, a , and the feed concentration is found to be:

$$\frac{a_1}{a_2} = \left(\frac{C_{o1}}{C_{o2}} \right)^{1/2} \quad (22)$$

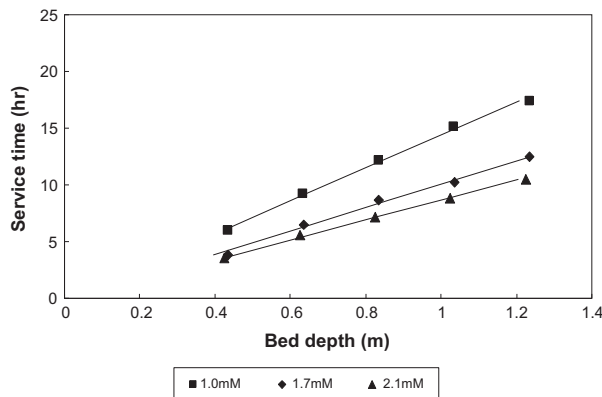


Fig. 8. Modified BDST plot for Ni ion exchange with different feed concentrations (flowrate = 180 ml/min, mean $d_p = 725 \mu\text{m}$, 10% breakthrough).

4.3.3.3. *Change of percentage breakthrough.* Tables 10 and 11 show the bed performance with different percentage breakthrough for the three metal ions based on original and modified BDST models, respectively. In general, the modified BDST model can result in an improvement of up to 14% in the SSE. Fig. 9 shows the modified BDST plot for Ni ion exchange with different percentage breakthroughs to illustrate the effect on the bed performance.

As the breakthrough curves for the three metal ion exchange systems are rather steep and show basically constant-pattern behaviour, it implies that the mass transfer zone is short. As shown in Tables 10 and 11, the slopes and in turn the bed capacities, N_o , of both

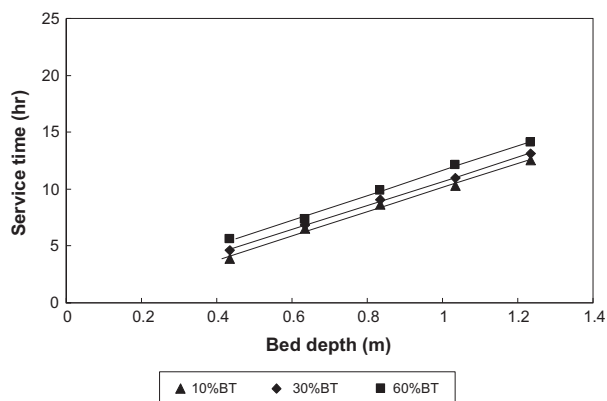


Fig. 9. Modified BDST plot for Ni ion exchange with different percentage breakthrough ($C_o = 1.5$ mM, flowrate = 180 ml/min, mean $d_p = 725$ μ m).

the BDST plots and modified BDST plots are fairly constant regardless of the percentage breakthrough. This concurs well with the Bohart–Adam’s equation in which the percentage breakthrough, i.e. C_b/C_o , should not affect the slope of the BDST plots.

Table 11 reveals that when the percentage breakthrough is high, the rate constant, a , increases to a very high value and the term $(1 - \exp(-a\sqrt{t}))$ of the modified BDST diminishes to 1. That means N_t is always N_o at high percentage breakthrough and the modified BDST model reduces to the original BDST model. The reason for this is because the original BDST model equation assumes a rectangular isotherm and N_o is assumed to be constant. Whereas, in reality, the isotherms for the three metal ions are a bit curved. Therefore, if the selected breakthrough solute concentration, C_b , is rather small, the corresponding exchange capacity will be less than q_{max} at the horizontal part of the isotherm. This is reflected from a small value of a . However, if the percentage breakthrough is higher, the original BDST model’s assumption is valid and thus the term $(1 - \exp(-a\sqrt{t}))$ becomes insignificant.

The critical bed depth, Z_o , decreases with the increase in the percentage breakthrough as indicated in Eq. (13). A higher percentage breakthrough would mean that a higher solute concentration in the effluent

is allowed and thus, a smaller minimum bed depth is required to keep the effluent concentration to below the breakthrough limit. Table 11 shows that when the percentage breakthrough is 30% or above, the critical bed depth, Z_o , is negative, which implies that at $t = 0$, the bed depth, Z , is always above the minimum bed depth required to keep effluent concentration to below the breakthrough limit.

4.3.3.4. Change of particle size. Normally, the resin size is fixed by the resin manufacturer. Thus, the particle size, unlike system flowrate or feed concentration, is not a system parameter that can be changed easily. Nevertheless, it is worthwhile to have a look at the effect of particle size on the ion exchange process. Tables 12 and 13 show the bed performance with three different particle sizes for the Ni ion exchange based on original and modified BDST models, respectively. Again, the modified BDST model, can result in an improvement of up to 17% in the SSE. Fig. 10 illustrates the effect of particle size on the bed performance of Ni ion exchange.

As shown in Table 13, the rate constant, a , is found to be inversely proportional to the mean particle size:

$$\frac{a_1}{a_2} = \frac{d_{p2}}{d_{p1}} \quad (23)$$

The increase of the rate constant, a , with the decrease in mean particle size suggests an improvement in the mass transfer in the finer resin particles. Smaller particles have narrower void space which results in higher Reynold’s number, reducing the film resistance. Smaller particles also provide more specific external surface area which reduces the external mass transfer resistance. Moreover, a shorter diffusion path in smaller particles results in faster penetration of the metal ions into the interior of the resin particles.

Theoretically, resin particle size should have very little effect on the slope of the BDST plots as well as the saturation capacity. However, Tables 12 and 13 reveal that smaller particle sizes have a slightly higher saturation capacity. This may be because large resins have more functional sites that are difficult to be

Table 10
BDST analysis for different percentage breakthrough ($C_o = 1.5$ mM, mean $d_p = 725$ μ m, flowrate = 180 ml/min)

Metal ion	Percentage breakthrough	Slope, m (h/m)	Y-intercept, c (h)	X-intercept, Z_o (m)	N_o (g/l)	SSE ($\times 10^{-3}$)
Ni	10	10.6	−0.49	0.05	33.6	2.63
Ni	30	10.5	0.15	−0.01	33.3	0.35
Ni	60	10.8	0.78	−0.07	34.3	1.20

Table 11

Modified BDST analysis for different percentage breakthrough ($C_o = 1.5$ mM, mean $d_p = 725$ μ m, flowrate = 180 ml/min)

Metal ion	Percentage breakthrough	m' (h/m)	c' (h)	a ($h^{-0.5}$)	Z_o (m)	N_o (g/l)	SSE ($\times 10^{-3}$)	New SSE/old SSE
Ni	10	10.5	-0.23	1.54	0.02	33.0	2.43	0.92
Ni	30	10.4	0.35	1.55	-0.03	32.9	0.30	0.86
Ni	60	10.8	0.78	7.11	-0.07	34.3	1.20	1.00

Table 12

BDST analysis for different particle size ($C_o = 1.5$ mM, flowrate = 180 ml/min, 10% breakthrough)

Metal ion	d_p (μ m)	Slope, m (h/m)	Y-intercept, c (h)	X-intercept, Z_o (m)	N_o (g/l)	SSE ($\times 10^{-3}$)
Ni	850	10.8	-1.79	0.17	34.4	0.80
Ni	650	11.4	-1.15	0.10	36.1	0.67
Ni	525	11.4	-0.73	0.06	36.2	0.33

Table 13

Modified BDST analysis for Ni using different particle size ($C_o = 1.5$ mM, flowrate = 180 ml/min, 10% breakthrough)

d_p (μ m)	m' (h/m)	c' (h)	a ($h^{-0.5}$)	Z_o (m)	N_o (g/l)	SSE ($\times 10^{-3}$)	New SSE/old SSE
850	10.4	-0.33	0.76	0.03	33.0	0.71	0.87
650	11.0	-0.30	1.00	0.03	34.9	0.60	0.89
525	11.1	-0.25	1.25	0.02	35.2	0.27	0.83

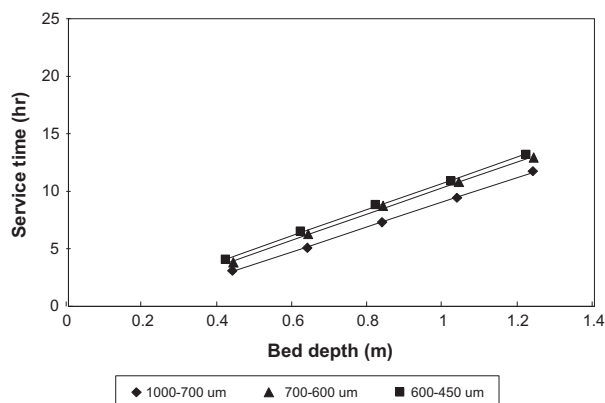


Fig. 10. Modified BDST plot for Ni ion exchange with different particle sizes ($C_o = 1.5$ mM, flowrate = 180 ml/min, 10% breakthrough).

accessed by metal ions due to greater steric hindrance effect and the diffusion of ions in the resin phase may be hindered by the chemical reactions, like the dissociation–association and complexation of the fixed exchange sites of the resin [42–44]. Helfferich (1965) describes eleven different ion exchange processes which are accompanied by chemical reactions between fixed-, counter- and co-ions and inhibit the diffusion process of the metal ions to the resin sites [45].

5. Conclusion

The ion exchange of nickel ions from water has been studied in a series of fixed bed experiments. The breakthrough characteristics of the breakthrough curves have been successfully correlated using a modified BDST equation. The original BDST equation did not correlate the data very well as the original Bohart-Adams BDST model was based on surface adsorption reaction only. Our modified BDST model incorporates a time-dependent adsorption capacity term, N_t , as opposed to an independent capacity term, N_0 . The modified BDST model gave excellent correlation to the experimental results.

References

- [1] W.J.M. Dediétrich, F.P. Reinhard, Waste minimization and recovery technologies, *Met. Finish.* 105(10) (2007) 715–742.
- [2] T.H. Eom, C.H. Lee, J.H. Kim, C.H. Lee, Development of an ion exchange system for plating wastewater treatment, *Desalination* 180(1–3) (2005) 163–172.
- [3] Y. Hannachi, A. Hannachi, The efficiency of the flotation technique for the removal of nickel ions from aqueous solution, *Desalin. Water Treat.* 6(1–3) (2009) 299–306.
- [4] H.J. Mansoorian, A. Rajabizadeh, E. Bazrafshan, A.H. Mahvi, Practical assessment of electrocoagulation process in removing nickel metal from aqueous solutions using iron-rod electrodes, *Desalin. Water Treat.* 44(1–3) (2012) 29–35.
- [5] A. Talebi, T.T. Teng, A.F.M. Alkarkhi, I. Norli, L.W. Low, Optimization of nickel removal using liquid-liquid extraction and response surface methodology, *Desalin. Water Treat.* 47 (1–3) (2012) 334–340.

- [6] Y. Hannachi, N.A. Shapovalov, A. Hannachi, Adsorption of nickel from aqueous solution by the use of low-cost adsorbents, *Desalin. Water Treat.* 12(1–3) (2009) 276–283.
- [7] H.J. Su, Z.X. Wang, W.T. Tan, Adsorption of Ni (2+) on the surface of molecularly imprinted adsorbent from *Penicillium chrysogenum* mycelium, *Biotechnol. Lett.* 25(12) (2003) 949–953.
- [8] W.T. Tan, C.K. Lee, K.L. Ng, Column studies of copper (2+) and nicked (2+) ions sorption on palm pressed fibres, *Environ. Technol.* 17 (1996) 621–628.
- [9] G. Wang, A. Li, M. Li, Sorption of nickel ions from aqueous solutions using activated carbon derived from walnut shell waste, *Desalin. Water Treat.* 16(1–3) (2010) 282–289.
- [10] K.K.H. Choy, G. McKay, Sorption of metal ions from aqueous solution using bone char, *Environ. Int.* 31 (2005) 845–854.
- [11] C.K. Ko, J.F. Porter, G. McKay, Mass transport model for the fixed bed sorption of metal ions on bone char, *Ind. Eng. Chem. Res.* 42 (2003) 3458–3469.
- [12] J. Jangbarwala, Ion exchange resins for metal finishing wastes, *Met. Finish.* 95(11) (1997) 33–34.
- [13] H. Eccles, Ion exchange—future challenges/opportunities in environmental clean-up, Proceedings of the Ion-Ex '95 Conference: Progress in Ion Exchange—Advances and Applications, Wrexham, Royal Society of Chemistry, Information Services, Cambridge, 1995, pp. 245–259.
- [14] S.J. Allen, P. Brown, O. Flynn, G. McKay, An evaluation of single transfer models on the sorption of metal ions by peat, *J. Chem. Technol. Biotechnol.* 45(3) (1992) 173–189.
- [15] G. McKay, B. Vong, J.F. Porter, Isotherm studies for the sorption of metal ions on to peat, *Adsorpt. Sci. Technol.* 16(1) (1998) 51–66.
- [16] Y.S. Ho, G. McKay, Competitive sorption of copper and nickel ions from aqueous solutions using peat, *Adsorption* 5 (1999) 405–417.
- [17] Y.S. Ho, G. McKay, The kinetics of sorption of divalent metals onto sphagnum moss peat, *Water Res.* 34 (2000) 735–742.
- [18] Y.S. Ho, G. McKay, G. Wase, C.F. Forster, Study of the sorption of divalent metal ions on to peat, *Adsorpt. Sci. Technol.* 18 (2000) 639–650.
- [19] Y.S. Ho, J.F. Porter, G. McKay, Equilibrium isotherm studies for the sorption of divalent metal ions onto peat: Copper, nickel and lead single component systems, *Water Air Soil Pollut.* 141 (2002) 1–33.
- [20] A. Demirbas, E. Pehlivan, F. Gode, T. Altun, G. Arslan, Adsorption of Cu(2+), Zn(2+), Ni(2+), Pb(2+), and Cd(2+) from aqueous solution on Amberlite IR-120 synthetic resin, *J. Colloid Interface Sci.* 282(1) (2005) 20–25.
- [21] K.F. Lam, K.L. Yeung, G. McKay, Efficient approach for Cd²⁺ and Ni²⁺ removal and recovery using mesoporous adsorbent with tunable selectivity, *Environ. Sci. Technol.* 41 (2007) 3329–3334.
- [22] A. Ma, T.H. Shek, S.J. Allen, V.K.C. Lee, G. McKay, Removal of nickel from effluents by chelating ion exchange, *J. Chem. Technol. Biotechnol.* 83 (2008) 1623–1632.
- [23] A. Demirbas, E. Pehlivan, F. Gode, Adsorption of Cu(2+), Zn (2+), Ni(2+), Pb(2+), and Cd(2+) from aqueous solution on Amberlite IR-120 synthetic resin, *J. Coll. Interf. Sci.* 282(1) (2005) 20–25.
- [24] K.G. Ashurst, Thermodynamic aspects of chelating ion exchange resins, In: D. Naden, M. Streat (Eds), *Ion Exchange Technology*, Ellis Horwood, Chichester, pp. 189–200, 1984.
- [25] E. Arevalo, A. Fernandez, M. Rendueles, M. Diaz, Equilibrium of metals with iminodiacetic resin in binary and ternary systems, *Solvent Extr. Ion Exch.* 17(2) (1999) 429–454.
- [26] C. Eger, W.M. Anspach, J.A. Marinsky, The co-ordination behavior of Co, Ni, Cu and Zn in a chelating ion-exchange resin I-II, *Ind. Eng. Chem. Fundam.* 30 (1968) 1899–1909.
- [27] A.K. Sengupta, Y. Zhu, D. Hauze, Metal (II) ion binding onto chelating exchangers with nitrogen donor atoms: Some new observations and related implications, *Environ. Sci. Technol.* 25 (1991) 481–488.
- [28] F.G. Helfferich, Ion-exchange kinetics. A nonlinear diffusion problem. II. Particle diffusion controlled exchange of univalent and bivalent ions, *J. Chem. Phys.* 29(5) (1958) 1064–1069.
- [29] F.G. Helfferich, Ion exchange kinetics—Evolution of a theory, *Mass Transfer and Kinetics of Ion Exchange*, NATO ASI, Series E, No.71 (1983).
- [30] F.G. Helfferich, *Ion Exchange*, Dover Publications, New York, NY, 1995.
- [31] G.S. Bohart, E.Q. Adams, Some aspects of the behavior of charcoal with respect to chlorine, *J. Chem. Soc.* 42 (1920) 523–529.
- [32] R.A. Hutchins, New method simplifies design of activated carbon systems, *Chem. Eng.* 80 (1973) 133–138.
- [33] C.K. Ko, J.F. Porter, G. McKay, Mass transport model for the fixed bed sorption of metal ions on bone char, *Ind. Eng. Chem. Res.* 42 (2003) 3458–3469.
- [34] J.C. Crittenden, W.J. Weber, Jr. Predictive model for design of fixed-bed adsorbents: Single-component model verification, *J. Environ. Eng. Division ASCE* 104(EE22) (1978) 433–443.
- [35] G. McKay, Mass transfer processes during the adsorption of solutes in aqueous solutions in batch and fixed bed adsorbents, *Chem. Eng. Res. Des.* 62 (1984) 235–246.
- [36] W.J. Weber, Jr., C.K. Wang, A microscale system for estimation of model parameters for fixed-bed adsorbents, *Environ. Sci. Technol.* 21 (1987) 1096–1102.
- [37] G. McKay, M.J. Bino, Adsorption of pollutants on to activated carbon in fixed beds, *J. Chem. Technol. Biotechnol.* 37(2) (1987) 81–93.
- [38] E.H. Smith, W.J. Weber Jr., Evaluation of mass transfer parameters for adsorption of organic compounds from complex organic matrices, *Environ. Sci. Technol.* 23 (1966) 713–722.
- [39] E.J. Wilson, C.J. Geankoplis, Liquid mass transfer at very low Reynolds numbers in packed beds, *Ind. Eng. Chem. Fundam.* 5 (1966) 9–12.
- [40] G. McKay, Basic dye adsorption on activated carbon, *Water Air Soil Pollut.* 12 (1979) 307–317.
- [41] M.F.F. Sze, V.K.C. Lee, G. McKay, Simplified fixed bed column model for adsorption of organic pollutants using tapered activated carbon columns, *Desalination* 218 (2008) 323–333.
- [42] W. Holl, H. Sontheimer, Ion exchange kinetics of the protonation of weak acid ion exchange resins, *Chem. Eng. Sci.* 32 (1977) 755–762.
- [43] M. Streat, Kinetics of slow diffusing species in ion exchangers, *React. Polym.* 2 (1984) 79–91.
- [44] H. Yoshida, T. Kataoka, S. Fujikawa, Kinetics in a chelate ion exchanger-II. Experimental, *Chem. Eng. Sci.* 41 (1986) 2525–2530.
- [45] F. Helfferich, Ion-exchange kinetics. V. Ion exchange accompanied by reactions, *J. Phys. Chem.* 69(4) (1965) 1178–1187.